Design and implementation of a 3-D mapping system for highly irregular shaped objects with application to semiconductor manufacturing

Vivek A. Sujan
Steven Dubowsky
Massachusetts Institute of Technology
Department of Mechanical Engineering
Cambridge, Massachusetts 02139

Abstract. The basic technology for a robotic system is developed to automate the packing of polycrystalline silicon nuggets into fragile fused silica crucible in Czochralski (melt pulling) semiconductor wafer production. The highly irregular shapes of the nuggets and the packing constraints make this a difficult and challenging task. It requires the delicate manipulation and packing of highly irregular polycrystalline silicon nuggets into a fragile fused silica crucible. For this application, a dual optical 3-D surface mapping system that uses active laser triangulation has been developed and successfully tested. One part of the system measures the geometry profile of a nugget being packed and the other the profile of the nuggets already in the crucible. A resolution of 1 mm with 15-KHz sampling frequency is achieved. Data from the system are used by the packing algorithm, which determines optimal nugget placement. The key contribution is to describe the design and implementation of an efficient and robust 3-D imaging system to map highly irregular shaped objects using conventional components in context of real commercial manufacturing processes. [DOI: 10.1117/1.1474438]

Subject terms: 3-D surface mapping; laser triangulation; silicon nuggets; semiconductor manufacturing.

Paper 010142 received Apr. 23, 2001; revised manuscript received Dec. 28, 2001; accepted for publication Dec. 31, 2001.

1 Introduction

The requirements for growing large single device-grade semiconductor crystals are very stringent. Extraordinarily low impurity levels, on the order of 1 part in 10 billion, require careful handling and treatment of the material at each step of the manufacturing process. During the Czochralski (melt pulling) semiconductor wafer production process (also known as the CZ process), highly irregular shaped polycrystalline silicon nuggets (Fig. 1) are packed (charged) into large fused quartz crucibles.[1,2] The nuggets range in weight from a few grams to about 600 grams. Avoiding contamination, protecting the crucible from damage, and following complex packing density rules are key constraints during the process.[2] Once packed, these crucibles are placed in ovens, in which the CZ melt pulling process occurs. The extruded semiconductor ingots are then sliced into wafers from which semiconductor chips are etched. Currently 45.7-cm-diam crucibles, which are packed manually, are being replaced by much larger (more than 91.5 cm diam) crucibles, for use in the upcoming fabrication of a new generation of 300-mm-diam wafers.[2,3] In these crucibles, manual packing is neither ergonomic nor practical. Automation has the potential benefit of reducing cost, achieving greater packing consistency, and reducing packing time. Previous studies have shown that because each nugget has a unique size and shape, and because of strict packing rules, fixed automation was not feasible.[1,2,4]

The large variance in size and weight, the irregular shape of the nuggets (see Fig. 1), and the strict process requirements result in four key technical challenges to automate the crucible packing process with a robotic system. First, the nuggets are difficult to grasp. Second, nuggets must be placed in accordance with their geometry and the

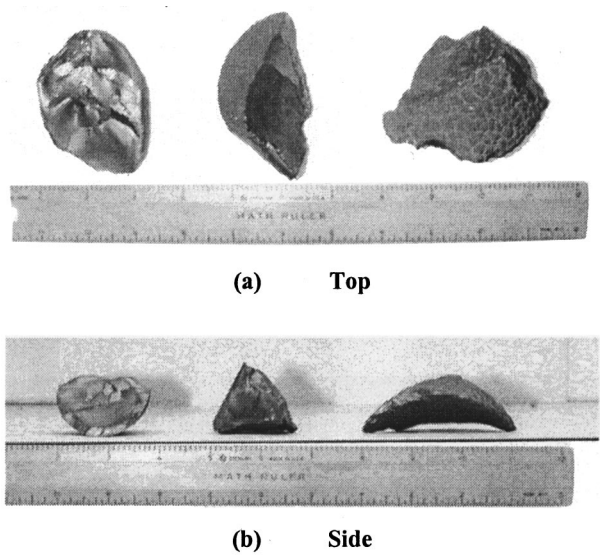

Fig. 1 Typical polycrystalline silicon nuggets: (a) top and (b) side.

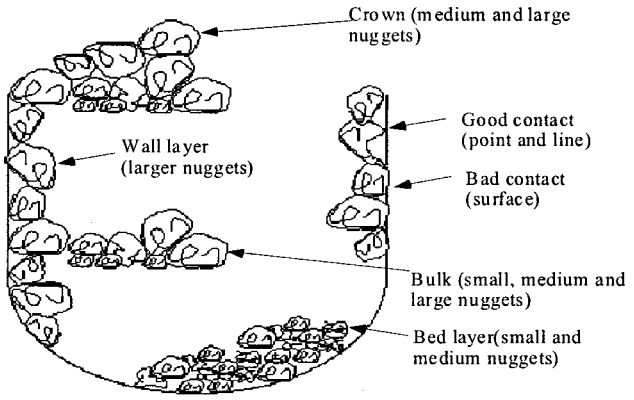

(a) Charging constraints

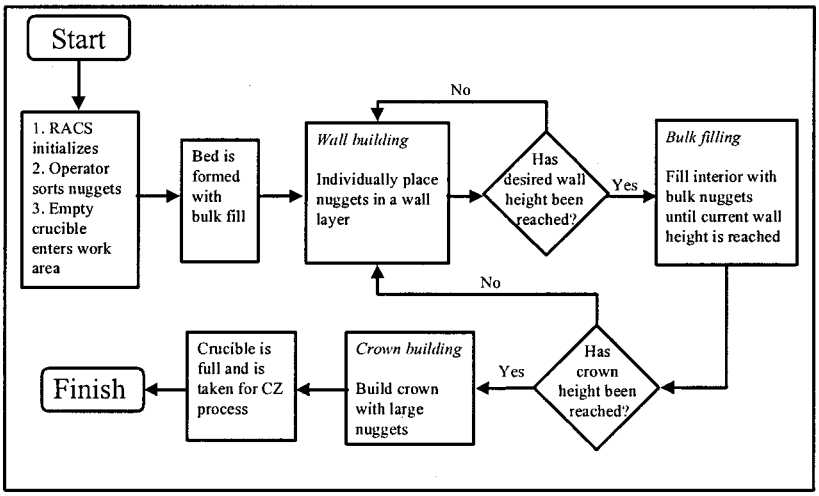

(b) Charging process

Fig. 2 Typical crucible charging: (a) charging constraints and (b) charging process.

proper set of packing rules within the process specifications. Hence each nugget and crucible surface must be scanned rapidly and accurately to get surface profiles before a nugget is placed. Third, the planning system must use this profile information to determine the optimal placement of a nugget in a crucible. Determining the best location to place each nugget is necessary due to the importance of the packing density and complex process constraints. Finally, the irregularly shaped and stiff nuggets must be carefully placed against the fragile quartz crucible wall without scratching and contaminating the process. They must also be carefully placed against other nuggets in the process without disturbing the existing structure. This is usually accomplished by handling the larger nuggets individually. Figure 2 shows the schematic of a packed crucible. The packing rules are set by the technology and the stringent traditional CZ crystal production rules. These packing rules require that the nuggets be placed in layers. Packing is initiated with a bed layer formed by smaller, gravel-sized nuggets. The following nugget layers consist of larger wall nuggets and internal smaller bulk nuggets. Alternate filling of the bulk and wall nuggets eventually results in a full crucible. Finally, packing is completed with a crown of larger nuggets. Figure 3 shows the system concept developed in this study.[1,2] During the stratified packing, nuggets are acquired one at a time by the manipulator and passed over the nugget scanner to obtain its surface profile. Simultaneously, the crucible surface profile is mapped by an overhead vision system. A packing algorithm applies this vision data to compute an ideal position for the nugget. The system timing is critical to the economic viability of the system. To stay competitive with human packing, individual nuggets forming the wall and the crown need to be placed one every 10 sec.[2,3] In such a system, the operator will only be responsible for opening bags and sorting nuggets.

A key technical component is a vision system to provide the 3-D surface geometries of the individual nuggets before they are placed in the crucible and of the nuggets that have already been packed.[4] Machine vision providing 3-D surface geometry information has been widely studied and applied.[5–13] The CZ process contains constraints, such as a complex environment, cost, and compactness, which make the practical design of 3-D surface geometry acquisition

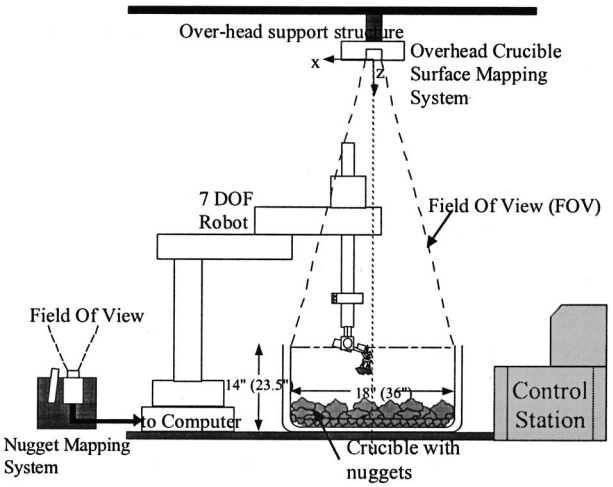

Fig. 3 Crucible charging system layout.

very challenging. The design of a 3-D vision system using active laser triangulation with CCD cameras to meet the stringent requirements of the CZ process is presented. One system element is for surface mapping of the landscape of nuggets in the crucible, and the second for the individual nugget mapping. We outline the design, implementation, and calibration of the systems. We also present experimental results that show it can meet the requirements of CZ process automation.

2 Vision System Design

2.1 *System Requirements*

The vision system of the crucible packing system gathers the environmental data that are required by the packing algorithm. After being grasped, the nugget shape and orientation, and the internal surface profile of the crucible, are measured and processed by the computer vision system. The packing algorithm utilizes the three-dimensional data or a range map of the profiles for the nugget and the internal crucible surface, to determine a satisfactory location of the nugget within the current crucible state. The primary considerations for an industrial vision system are cost, speed, accuracy, and reliability. To pay for itself, an industrial vision system must outperform the human labor it replaces in all of these categories.[11,13,14] In most cases, the vision system must perform a real-time analysis of the image to compete with humans. Table 1 summarizes the system requirements for the crucible charging vision system as determined by the factory and charge requirements.[1,2]

2.2 *Range Sensing*

Range-imaging sensors collect three-dimensional coordinate data from visible surfaces in a scene, and can be used in a wide variety of automation applications, including object shape acquisition, bin picking, robotic assembly, inspection, gauging, mobile robot navigation, automated cartography, medical diagnosis (biostereometrics), etc.[11,14–17] The image data points explicitly represent scene surface geometry as sampled points. The inherent problems of interpreting 3-D structure in other types of imagery (where 3-D data is obtained based on 2-D cues) are not encountered in range imagery, although most low level problems, such as filtering, segmentation, and edge detection, remain. Most optical techniques for obtaining range images are based on one of the five principles: triangulation, holographic interferometry (phase shift measurement), radar (time of flight), lens focus, and moiré techniques.[6,7,15,18] A detailed review in which several of these methods are discussed and compared has been published.[7,10–12] Table 2 lists the main comparison features of these five methods. All these methods suffer some limitations, such as blind regions, computational complexity, highly textured or structured scenes, surface orientation, and/or spatial resolution.[10,15] Active triangulation eliminates many problems provided that an intense enough light source is available. It can capture the third dimension through model-free range measurement. This can be very useful in 3-D scene analysis. It can resolve many of the ambiguities of interpretation arising from lack of correspondence between object boundaries and inhomogeneities of intensity, texture, and color found in other methods.[6,7,10,12,14]

Table 1 Vision system requirements.

1. High Accuracy	Approximately 1 mm
2. Fast—for automation	Nugget mapping ~2 to 3 s
	Crucible surface mapping ~4 to 5 s
3. Obtrusiveness	No interference with robotic system
	Minimum change in factory ambient lighting
4. System Interfacing	Suitable data representation for packing
5. Costs	Factory system vision costs ⩽$20,000

2.3 *Active Triangulation*

One of the most commonly seen methods for the acquisition of three-dimensional data is the laser triangulation method.[7–9,15,19,20] A structured light source, such as point, line, or color coding, is used to illuminate the object and either one or more cameras (possible for stereoscopic vision systems) detect the reflected light (see Fig. 4). The location and orientation of the cameras (determined precisely with calibration) yields an equation that determines the 3-D location of the illuminated point. By scanning the entire object, a 3-D map of the object can be acquired.

2.3.1 *Model 1: Point-wise triangulation using two stereoscopic cameras*

Figure 5 is an orthographic view of the system. The origin of the world coordinate system is set at the front node of the lens of camera 1. The X axis passes through the front node of the lens of camera 2. The Z axis is positive in the direction of the laser beam, which originates between the two cameras. In this design, the position/orientation of the laser is not critical but provides for a simple solution to the stereo matching problem.

The v axis of the detector is assumed to be parallel to the world Y axis (though this requirement can be mathematically relaxed). Optimization of the combined field of view requires that $\theta_2 = -\theta_1 = 45$ deg. The distances between back nodes of the lenses and the detectors are the principal focal distances f_1 and f_2. The 2-D coordinates

Table 2 Qualitative comparisons of range sensing methodologies.

	Active/passive triangulation	Holographic interferometry	Radar: TOF, AM, FM	Lens focus	Moiré Techniques: projection, shadow, single frame + ref, multiple frame
Resolution/ accuracy	>2.5 μm (with specific hardware)	>3 μm (0.4 nm theoretical)	⩾100 μm	>1 mm	>11 μm
Data acquisition rate	<10-M pixels/s	<1-K points/s	⩽100-K pixels/s	<60-K pixels/s	<100-K pixels/s
Depth of field	O(mm)→ O(10 meters)	O(mm)→O(100 meters)	⩾O(mm)	O(100 mm) →O(meter)	>O(100 mm)
Limitations	Detector noise, data processing power	alignment, system noise	High res. + data acq. rate⇒small depth of field	lens quality/ positioning/ measuring	only for smooth surfaces high resolution ⇒small depth of view

measured on the image planes are (u_1,v_1) and (u_2,v_2) in the detectors' own coordinate systems. These can be transformed into vectors $\mathbf{R}_1$ and $\mathbf{R}_2$ in the world coordinate system with:

$$\vec{R}_1 = M_1 \vec{R}_1' \quad \text{and} \quad \vec{R}_2 = M_2 \vec{R}_2', \tag{1}$$

where

$$M_1 = \begin{bmatrix} \cos\theta_1 & 0 & -\sin\theta_1 \\ 0 & 1 & 0 \\ \sin\theta_1 & 0 & \cos\theta_1 \end{bmatrix}$$

and

$$M_2 = \begin{bmatrix} \cos\theta_2 & 0 & -\sin\theta_2 \\ 0 & 1 & 0 \\ \sin\theta_2 & 0 & \cos\theta_2 \end{bmatrix}. \tag{2}$$

And $\mathbf{R}_1'$ and $\mathbf{R}_2'$ are in the detector coordinate systems:

$$\vec{R}_1' = \begin{Bmatrix} u_1 \\ v_1 \\ f_1 \end{Bmatrix} \quad \text{and} \quad \vec{R}_2' = \begin{Bmatrix} u_2 \\ v_2 \\ f_2 \end{Bmatrix}. \tag{3}$$

In theory, extensions of $\mathbf{R}_1$ and $\mathbf{R}_2$ should intersect each other because they are directions of light rays that come from the same light source located at **p** (Fig. 5). In practice, any misalignment or error in the system can result in skew. The vector **e** is defined to be the skew vector such that $|\mathbf{e}|$ is

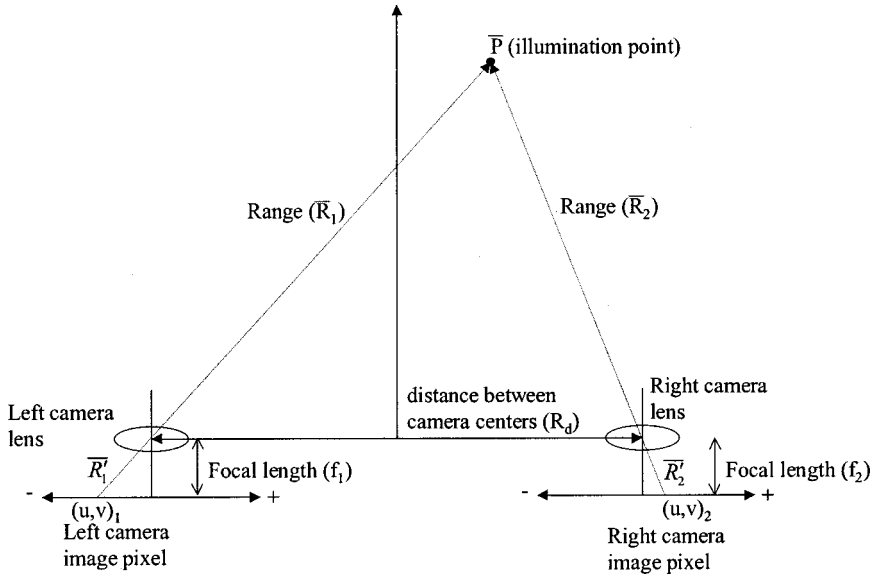

Fig. 4 General triangulation layout.

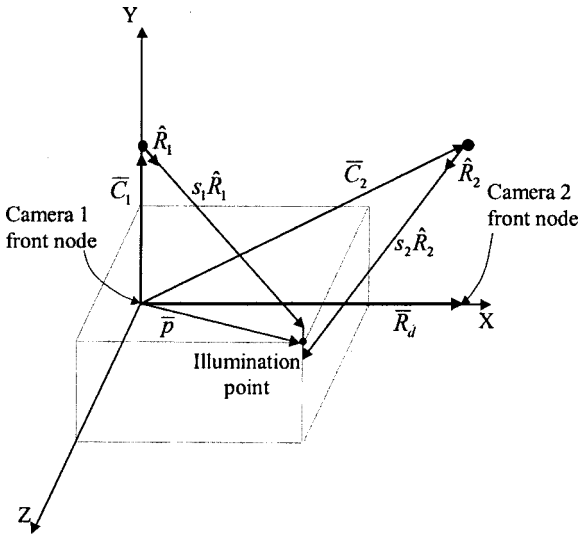

Fig. 5 Orthographic view triangulation using two stereoscopic cameras.

the shortest distance between the two lines. To find **e**, we define:

$$\mathbf{e}(S_1,S_2)=S_1\mathbf{R}_1-S_2\mathbf{R}_2-\mathbf{R}_d\,. \tag{4}$$

Minimizing $\{e(S_1,S_2).\ e(S_1,S_2)\}$ with respect to S_1 and S_2 (by taking partial derivatives) gives:

$$S_1=\frac{(\vec{R}_1,\vec{R}_d)(\vec{R}_2,\vec{R}_2)-(\vec{R}_2,\vec{R}_d)(\vec{R}_1,\vec{R}_2)}{(\vec{R}_1,\vec{R}_1)(\vec{R}_2,\vec{R}_2)-(\vec{R}_1,\vec{R}_2)(\vec{R}_1,\vec{R}_2)}$$

and

$$S_2=\frac{(\vec{R}_2,\vec{R}_d)(\vec{R}_1,\vec{R}_1)-(\vec{R}_1,\vec{R}_d)(\vec{R}_1,\vec{R}_2)}{(\vec{R}_1,\vec{R}_2)(\vec{R}_1,\vec{R}_2)-(\vec{R}_2,\vec{R}_2)(\vec{R}_1,\vec{R}_1)}, \tag{5}$$

e can thus be calculated. The coordinates of the spot **p** are defined to be at the center of **e**, giving:

$$\mathbf{p}=1/2(S_1\mathbf{R}_1+S_2\mathbf{R}_2+\mathbf{R}_d). \tag{6}$$

Since the system can determine the 3-D coordinates of a point anywhere in the combined field of view (FOV), and measure points in any order, it is possible to analyze the data stream from the system during acquisition and adaptively scan the light spot in response, allowing for data oversampling and the collection of spatially dense data in regions of interest.[15] The resolution, based on the nominal viewing volume, is found to be:

$$\frac{\vec{R}_d/2}{\text{Detector resolution}} \tag{7}$$

2.3.2 *Model 2: Point-wise triangulation using one camera*

The basic design is shown in Fig. 6.[20] A beam of light originates from position d along the X axis, projects at an angle θ_0, and defines a reference point $(d/2,\ell)$ that is used for calibration. At the origin, a lens of focal length f, focuses the reflected light on a position sensor aligned parallel to the X axis and in focus at $-f\ell/(\ell-f)$ along the Z axis. It is assumed that the values of d, l, and f are known. Under rotation of an optical scanner, the light beam rotates to another angular position $\theta_0+\theta$ (θ is negative in Fig. 6). The spot of light on the position sensor moves from $df/(2l-2f)$ to location **p** due to the intersection of the projected light beam with the object surface at x,z. The relationship between the coordinates (x,z) and the parameters of the geometry is:

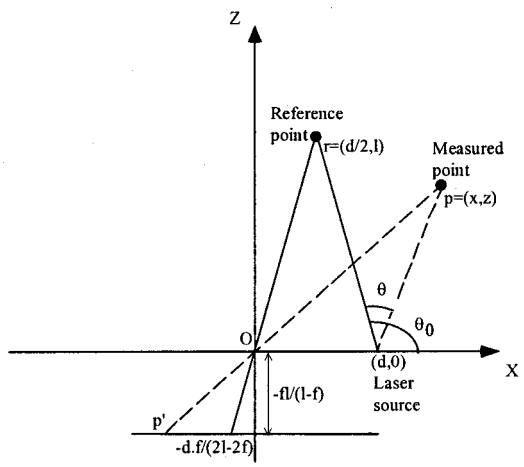

Fig. 6 Triangulation using one camera and reference point.

$$x=d\cdot p\left[p+\frac{f\cdot l(2l\cdot\tan\theta+d)}{(l-f)(d\cdot\tan\theta-2l)}\right]^{-1}$$

and

$$z=-d\left[\frac{p(l-f)}{f\cdot l}+\frac{2l\cdot\tan\theta+d}{d\cdot\tan\theta-2l}\right]^{-1}. \tag{8}$$

Equation (8) relies on accurate knowledge of the position of the reference point. Additionally, due to the optical nonlinearities of lenses, selection of an appropriate reference point can be difficult. An alternative, more accurate form of active triangulation using one camera is seen in Fig. 7. A single camera is aligned along a Z axis with the

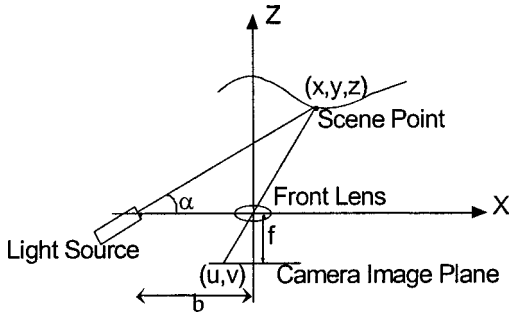

Fig. 7 Triangulation using one camera and laser pose.

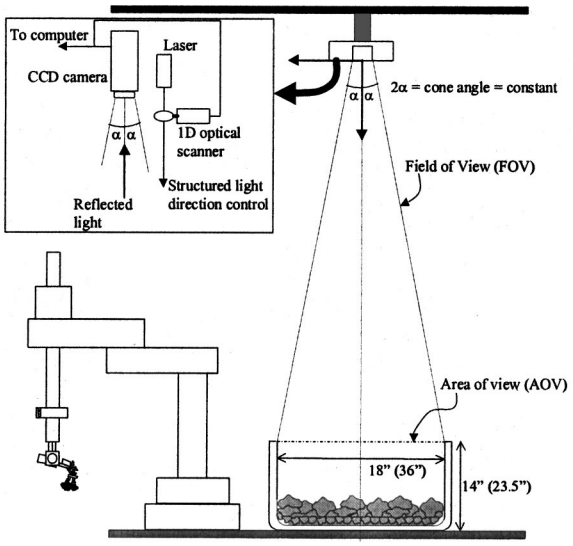

Fig. 8 Crucible mapping vision system layout.

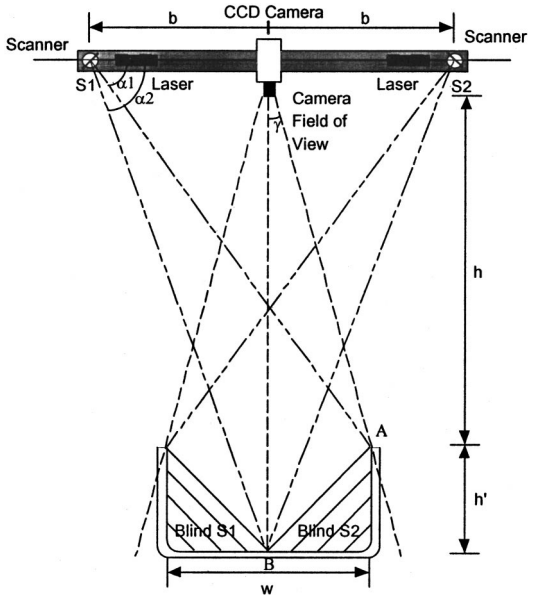

Fig. 9 Crucible surface mapping design parameters.

center of the front node of the lens located at (0,0,0), giving the origin of the camera coordinate frame. At a baseline distance b to the left of the camera (along the negative X axis) is a laser that projects a plane of light at a variable angle α relative to the X-axis baseline. The point (x,y,z) in the scene is projected onto the digitized image at the pixel (u,v)(see Fig. 7). The measured quantities (u,v) are used to compute the 3-D coordinates (x,y,z) of the illuminated scene point:

$$[x \;\; y \;\; z] = \frac{b}{f \cdot \cot(\alpha) - u}[u \;\; v \;\; f]. \tag{9}$$

For any given focal length f and baseline distance b, the resolution of this triangulation system is only limited by the ability to accurately measure the angle α and the image plane coordinates (u,v). The X and Y system resolution $(\delta X, \delta Y)$ is given by:

$$\frac{R}{\text{Detector resolution}}, \tag{10}$$

where R is the width of the projected image onto the detector. The depth resolution δZ, given an incident laser angle α, image width W, and n-pixel detector resolution, is given by:

$$\delta Z = (W \tan \alpha)/n. \tag{11}$$

The value of the resolution $(\delta X, \delta Y)$ may differ for the two image plane coordinates (u,v), as the detector resolution may not be identical for the two axes. Due to the added simplicity and larger field of view, this setup has been implemented on the laboratory prototype system, and is described in the following sections.

2.4 *System Layout—Crucible Surface Mapping*

The layout for the crucible surface mapping system is shown in Fig. 8. The crucible is scanned while the manipulator is out of the FOV. Scanning a surface involves projecting and moving laser light in the form a line (rather than a point) across the surface. The scanning consists of two phases: a low-resolution scan that is updated every 10 nugget placement cycles, and a high-resolution scan every nugget placement cycle in the area that was manipulated. The high-resolution scans are patched together to give a larger high-resolution map of the entire crucible. These maps are used to routinely monitor the crucible surface to identify any gross motions of nuggets falling out of place. Regions in the low-res map that do not match the high-res map (within a given tolerance) are remapped with a high resolution.

Based on the requirements outlined in Sec. 2.1, the crucible surface mapping system parameters outlined in Fig. 9 and Table 3 were developed. A crude/low-resolution global scan gives an XY resolution of 1.5 cm and takes one second to process for an 45.7-cm-diam crucible. Further resolution

Table 3 Crucible surface mapping design parameters.

Parameters	Lab Design
h	54 inches
h'	14 inches+crown
w	18 inches
b	36 inches
γ	9.5 degrees
$\alpha 1$	50.3 degrees
$\alpha 2$	63.4 degrees
Camera resolution (pixels)	500×500
Z resolution at A	1.1 mm
Z resolution at B	2.4 mm
X,Y resolution at A	0.9 mm
X,Y resolution at B	1.2 mm
Cost	$10,700

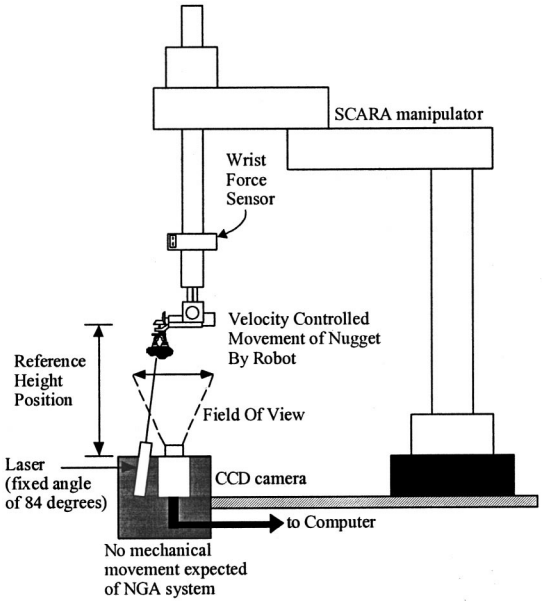

Fig. 10 Nugget surface mapping system layout.

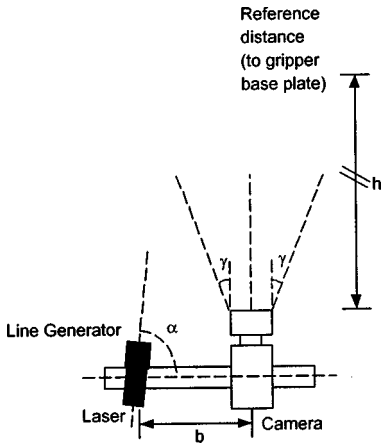

Fig. 11 Nugget mapping system design parameters.

improvement is achieved by allowing longer scan times. A higher resolution local scan (15-cm-wide band across the crucible) gives *XY* resolution of 1 mm and takes 4.5 s to process. All times are based on a standard video frame rate of 30 frames/s. These times are comparable to the times required for the manipulator actions of acquiring a new nugget and bringing it to the crucible of ~5.5 s.[12] Additionally, to avoid significant changes to the ambient lighting conditions, extracting the reflected laser light in the image requires subtracting an image with the laser on and one with the laser off. Laser intensity for such an operation is dependent on camera sensitivity, ambient lighting levels, nugget reflectivity, and proximity. For the laboratory system, a 5-mW laser was sufficient.

The crucible optical scanner uses a moving-magnet galvanometer. A moving-magnet motor has no saturation torque limit and very little electrical inductance. Thus extremely high torques can be generated very rapidly, an essential feature for systems requiring short step response times. The scanner controller is tuned for the inertial load of its mirror. A capacitive position detector within the scanner provides a differential current position control feedback. A latching digital circuit gives a maximum 16 bits of scanner control, equivalent to 10-μrad resolution.

2.5 *System Layout—Nugget Surface Mapping*

The prototype laboratory nugget surface mapping system is shown in Fig. 10. The manipulator grasps and carries the nugget over the vision system before it is placed in the crucible. It is scanned in real time as it moves across the camera. This requires careful synchronization of the manipulator motion and the nugget mapping system. The manipulator is required to maintain a constant linear velocity of the nugget across the camera FOV of 3 cm/s based on a 1-mm *XY* resolution, nominal nugget size of 7.5×7.5 cm, and 30 frames/s video rate. The nugget mapping system parameters are summarized in Fig. 11 and Table 4.

The process of nugget selection from the mapped image requires two primary considerations: 1. differentiating the nugget from the parts of the manipulator, and 2. differentiating the nugget from any overhanging gripper parts. Consideration 1. is resolved by setting the lowest visible part of the manipulator at a predefined reference height, with which data comparisons can be made and manipulator parts can be eliminated. Resolving consideration 2. can be more involved. The gripper is composed of three closely spaced, FDA grade vinyl B3-1, vacuum cups mounted on a manifold plate.[1,2] The manifold plate mounts to the end effector of the 7 DOF manipulator. Suction forces hold the nugget in place. The deformable shape of the gripper parts (suction cups) excludes feature extraction techniques. Differentiating the gripper based on reflection intensity properties can be misleading, as the cups get coated with a silicon dust layer during the charging process. The assumption that the gripper will always be occluded by the nugget in the field of view of the nugget mapping system is not a valid generalization, but true for a large fraction of the grasped nuggets.[2] The most reliable solution is to differentiate the gripper parts based on color mapping. The contrasting colors of the suction cups and the silicon nuggets, and the presence of ambient lighting make this option simple and robust to implement on the robotic system. Thus, the nugget mapping system with a color camera ignores measurements of reflected light originating from colored surfaces not matching a predefined palette.

Table 4 Nugget surface mapping design parameters.

Parameters	Lab/Factory Design
h (distance to nugget)	10 inches
B	1.7 inches
γ	12 degrees
α	84 degrees
Camera resolution in pixels	1000×1000
Z resolution	1.03 mm
X,Y resolution	0.11 mm
Cost	$4,200

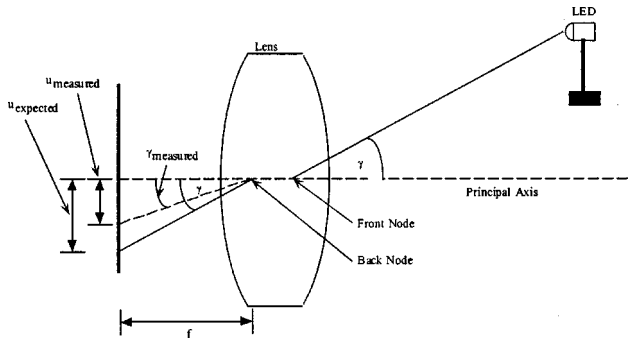

Fig. 12 Relationship between errors and angles.

3 Calibration

3.1 *Intrinsic Camera Calibration*

A perfect lens and a detector with perfectly linear characteristics would produce simple trigonometric relationships between the angle of an incoming light ray and the image plane coordinates (u,v) of the light source. In practice, imperfections in either of these elements will result in distortions.[21,22] The purpose of camera intrinsic calibration is to find and map the errors in image plane coordinates (u,v) due to the nonlinearities in lenses, detectors, and electronics.[15] These error measurements are used to compensate the measured values to produce accuracy equal to the resolution of the system. Given a known horizontal incident angle γ and vertical incident angle β between the light ray and the principal axis, and a known principal distance f, the ''expected'' image plane coordinate (u,v) can be calculated (see Fig. 12). Subtracting these from their actual values gives the error map value.

$$u_{\text{expected}}=f\cdot\tan\ \gamma,\ v_{\text{expected}}=f\cdot\tan\ \beta \tag{12}$$

$$E_u=u_{\text{expected}}-u_{\text{measured}}=f\cdot\tan\ \gamma-u_{\text{measured}} \tag{13}$$

$$E_u=v_{\text{expected}}-v_{\text{measured}}=f\cdot\tan\ \beta-v_{\text{measured}}. \tag{14}$$

This scheme assumes that E_u at $\gamma=0$ and E_v at $\beta=0$ are 0. For nonideal lenses, the focal length f would have to be mapped as an average value given by[15]:

$$f\approx\bar{f}=\frac{1}{n}\sum_n\left|\frac{u_{\text{measured}}}{\tan\ \gamma}\right|. \tag{15}$$

Using binary interpolation, an E_u and E_v can be looked up for every (u,v) pair, and compensation made. This error is generally important when system accuracy requirements are at submillimeter levels.

The hardware setup for this process is as follows. The camera lens system is mounted on a two-axis (pitch and yaw) goniometer. To square up the axes of the detector and goniometer, a high precision displacement indicator is placed against the lens mount and the camera rotated such that the detector experiences roll and yaw. By varying the angles and monitoring the displacement indicator, the detector axes can be aligned with the goniometer axes. Next, the zero position of the lens detector has to be found. This is the location where the principal axis of the lens intersects the detector. Again, with the camera oriented such that the detector experiences roll and yaw, an LED is placed in front of the camera. By rolling the detector and mapping the led trace, a circle center can be defined. This is the true zero, from which Eqs. (12), (13), and (14) are applied. Next, the camera is rotated (yaw) by 90 °, so that the detector can experience pitch and yaw. The LED is positioned such that at the camera home position (pitch and yaw angle of 0 °), an image is formed at the camera zero. This is achieved by manual adjustments of the LED until the image is formed at the desired location. Finally, by setting up the appropriate range of pitch and yaw angles, the calibration continues with the aid of Eqs. (12), (13), and (14).

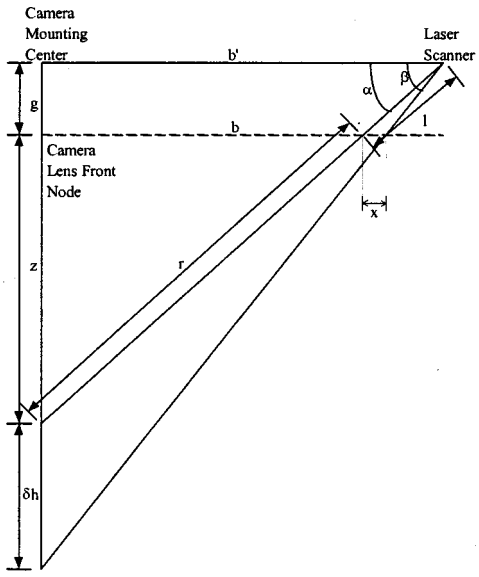

Fig. 13 Extrinsic calibration geometry for mapping system.

3.2 *Extrinsic Camera Calibration*

The extrinsic variables of the system that have to be predetermined are the focal length f and the intercamera laser distance b. Given an unknown lens focal length, intercamera laser distance b, and an unknown mounting orthogonality with respect to the ground, it is desired to be able to solve for the unknowns. The geometry shown in Fig. 13 yields six independent equations in six unknowns:

$$l=\frac{g}{\sin\ \alpha} \tag{16}$$

$$b=z\cdot\cot\ \alpha \tag{17}$$

$$b=b'-l\cdot\cos\ \alpha \tag{18}$$

$$z^2+b^2=r^2 \tag{19}$$

$$\frac{\sin(\beta-\alpha)}{\partial h}=\frac{\sin(\pi/2-\beta)}{r+l} \tag{20}$$

$$\frac{\sin(\pi-\beta)}{l}=\frac{\sin(\beta-\alpha)}{x}, \tag{21}$$

Table 5 Laboratory nugget mapping system extrinsic calibrated parameter values.

Optical image size (diameter)	6.477 mm
Half angle of view cone	20.6 deg
Effective focal length	8.616 mm

Table 6 Laboratory crucible mapping system extrinsic calibrated parameter values.

Effective focal length f	15.8 mm
Intercamera laser distance b	890 mm
Front node to mounting center g	153.03 mm
Object height	101.6 mm
Angle α, β	41.2, 44.5 deg

where g (measurable), α, β (predefined scan angles), and δh (object height) are known. The variable x is defined as the distance between the intersection points of the two incident rays, at angles α and β, with the extended camera lens front nodal plane. Tables 5 and 6 summarize the values obtained for the extrinsic parameters after solving Eqs. (16) through (21) for both the crucible surface mapping and nugget mapping systems. In this it is assumed that the incident angles can be found with the required accuracy.

3.3 *Timing Calibration*

As described in Sec. 2.5, timing between the nugget mapping system and the manipulator motion is critical. At an ideal frame rate of 30 Hz and a resolution of 1 mm, the manipulator is required to travel at 3 cm/s with a maximum allowable error of 0.5 mm/s for a scan time of 2.5 s. The primary source for errors in nugget position estimation arises in uncertainties in the video processing rates. This error can be resolved in one of three ways: 1. nugget mapping system manipulator coupling, where the manipulator is driven by interrupts provided by the nugget mapping system, reducing the problem to a robot position based control scheme; 2. off-line nugget mapping system timing, where the average processing rate of the nugget mapping system is measured off-line and then the known manipulator speed is used to infer nugget position; and 3. on-line nugget mapping system timing, where the time between individual frames is measured during scan and the known manipulator speed is used to obtain the correct nugget position. Due to its inherent simplicity (in computation and implementation) and accuracy, in this research the on-line nugget mapping system timing is used. Hence, any fluctuations in the frame rate or error in *a priori* knowledge of the frame rate is accounted for.

3.4 *Calibration of Coordinate Frames*

Finally, since all nugget manipulation is performed in the manipulator inertial coordinate frame, calibration is required for coordinate transformation between the imaging and manipulator systems. The crucible charging system is based on three coordinate frames: 1. the nugget mapping system coordinate frame; 2. the crucible mapping system coordinate frame, and 3. the manipulator coordinate frame. To successfully operate this system, the three coordinate frames (and images) must be related to a common reference frame, chosen as the manipulator coordinate frame.

Given a mapping system and the manipulator coordinate frames, the approach is to simplify the problem from that of six unknowns [three position (T_x, T_y, T_z) and three rotations (α, β, γ)] to that of three unknowns in position only. For a mapping system in some arbitrary position and orientation with respect to the manipulator, the general transformation matrix between the two coordinate frames is given by:

$$\begin{bmatrix} [R_{xyz}]_{3\times 3} & T_{xyz} \\ \vec{0} & 1 \end{bmatrix} = \begin{bmatrix} \cos\beta\cos\alpha & -\sin\gamma\sin\beta\cos\alpha - \cos\gamma\sin\alpha & \sin\gamma\sin\alpha - \cos\gamma\sin\beta\cos\alpha & T_x \\ \cos\beta\sin\alpha & \cos\gamma\cos\alpha - \sin\gamma\sin\beta\sin\alpha & -\sin\gamma\cos\alpha - \cos\gamma\sin\beta\sin\alpha & T_y \\ \sin\beta & \sin\gamma\cos\beta & \cos\gamma\cos\beta & T_z \\ 0 & 0 & 0 & 1 \end{bmatrix}, \quad (22)$$

where α, β, γ are the Euler angles for the rotational transformation between the two frames, and T_x, T_y, and T_z are the coordinates for the translational transformation between the two frames. If two points are known in the two coordinate frames, then by applying

$$\begin{bmatrix} x_{\text{camera}} \\ y_{\text{camera}} \\ z_{\text{camera}} \\ 1 \end{bmatrix} = \begin{bmatrix} [R_{xyz}] & T_{xyz} \\ \vec{0} & 1 \end{bmatrix} \cdot \begin{bmatrix} x_{\text{robot}} \\ y_{\text{robot}} \\ z_{\text{robot}} \\ 1 \end{bmatrix} \quad (23)$$

to the two sets of point coordinates, the six unknowns can be solved. In practice, solutions to transcendental equations require numerical methods. To simplify the problem, the crucible mapping system mounting is modified to fit a three rotational degree of freedom adjustment mechanism, consisting of a rotational table and a two-axis gimbal platform. This allows for roll, pitch, and yaw of the crucible mapping system. The crucible mapping system is then manually adjusted to eliminate rotational misalignments between the two coordinate frames. The general coordinate transformation problem simplifies to that of only translational transformation. For translational calibration, a single known point on the manipulator end effector is mapped by the imaging system. If this point is at a vector $\mathbf{x}_{\text{robot}}$ in the manipulator frame and $\mathbf{x}_{\text{camera}}$ in the imaging frame, then

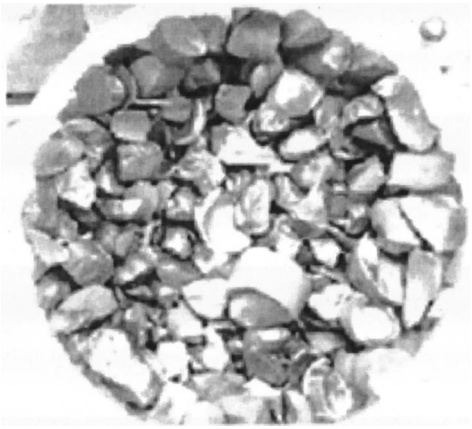

Fig. 14 Nugget field image.

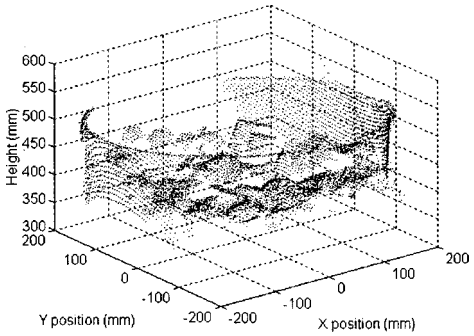

Fig. 15 Nugget field mapped profile.

the crucible mapping frame can be located with respect to the manipulator frame by vector triangulation, given by $\mathbf{x}_{\text{camera}}-\mathbf{x}_{\text{robot}}$. The transformation matrix simplifies to:

$$\begin{bmatrix} [R_{xyz}] & T_{xyz} \\ \vec{0} & 1 \end{bmatrix} = \begin{bmatrix} 1 & 0 & 0 & x_{\text{camera}}-x_{\text{robot}} \\ 0 & 0 & 0 & y_{\text{camera}}-y_{\text{robot}} \\ 0 & 0 & 1 & z_{\text{camera}}-z_{\text{robot}} \\ 0 & 0 & 0 & 1 \end{bmatrix}. \tag{24}$$

A similar method is used to calibrate the coordinate transformation of the nugget mapping system coordinate frame with respect to the manipulator inertial coordinate frame.

4 Results

4.1 *Crucible Mapping Results*

The primary purpose of the crucible mapping system is to provide a map of the nugget field already in the crucible, so that the manipulator-packing planner can determine an acceptable location for the next nugget. Figure 14 shows the raw image of a small nugget field, as might be seen in the crucible. Figure 15 shows a plot of the $z(x,y)$ values of this field provided by the crucible mapping system. A 15-KHz data acquisition rate is obtained, given a video rate of 30 frames/s and CCD resolution of 500×500 pixels on a Pentium 166-MHz system. With relatively low cost improvements in both resolution and computational speeds of the imaging hardware, the data acquisition rate can easily be substantially increased. The quantitative and independent precise measurement of a nugget field to check the crucible mapping system accuracy is difficult. However, estimates of the system's precision indicate that the mapping system should meet its required specifications. As discussed next, the quantitative evaluation of the accuracy of the nugget mapping system can be practically performed.

4.2 *Nugget Mapping Results*

A number of tests have been performed to evaluate the precision of the nugget mapping prototype system. In the simplest case, a calibration target consisting of 7 1-mm-step profile, machined onto a Delrin block, was scanned. The average error measured for those tests is ± 0.34 mm with σ of 0.12 mm (see Fig. 16). Recall that the accuracy requirement for the nugget mapping system is ± 1.0 mm.

The system was also evaluated using representative nuggets. Figure 17 shows one such nugget. The profile of this nugget obtained with the nugget mapping system is shown in Fig. 18. A section of this profile is shown in Fig. 19. Also shown in Fig. 19 is the error of the profile for this section compared to the profile measured with a coordinate mea-

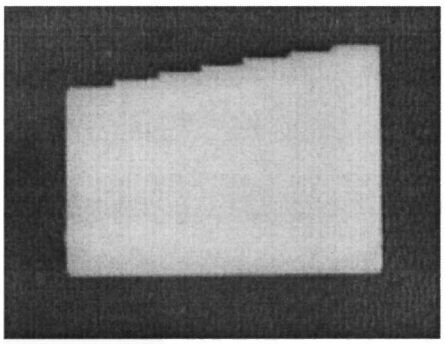

(a) Delrin block

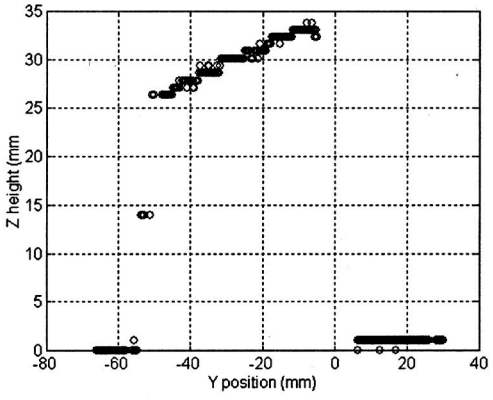

(b) mapped section profile

Fig. 16 Calibration target performance: (a) Delrin block and (b) mapped section profile.

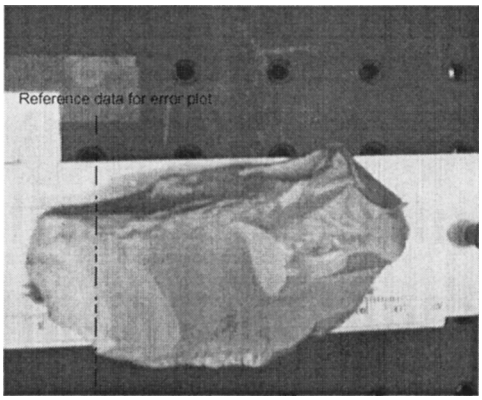

Fig. 17 A typical Nugget image.

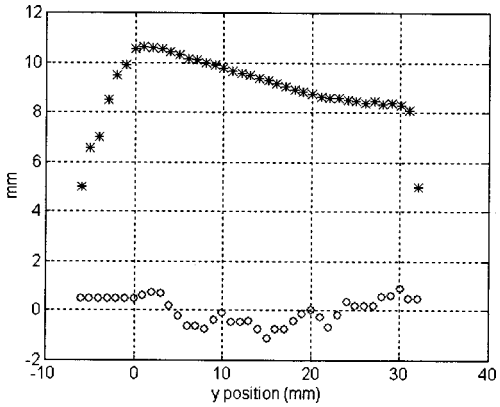

Fig. 19 Nugget mapped section profile: (*) profile and (o) error based on coordinate measuring machine data.

suring machine (CMM). The average error is ± 0.4 mm with σ of 0.2 mm. The maximum error seen here is approximately 1 mm, which could be partly an artifact of mismatching of the reference data on the mapped profile.

5 Laboratory System Integration

The laboratory system consists of a robot manipulator/control system, vision system, packing algorithm, and wrist/gripper system (see Fig. 20). The packing procedure plays a supervisory role in planning and assigning control to the major subsystems. This includes nugget acquisition, nugget scanning, crucible surface mapping, placement planning, nugget placement, and bulk filling.

To provide for accurate scheduling, the governing system communicates with the major subsystems, either across computers or across programs. It is recommended that a factory-level system be operated by a central workstation to maintain simplicity. For intercomputer communication, a series of asynchronous handshaking protocols have been developed for communication. These include:

- trigger nugget mapping module for nugget scan
- trigger crucible mapping module for crucible surface profiling
- trigger packing algorithm for image extraction and placement
- transfer nugget position and orientation placement coordinates to manipulator for placement.

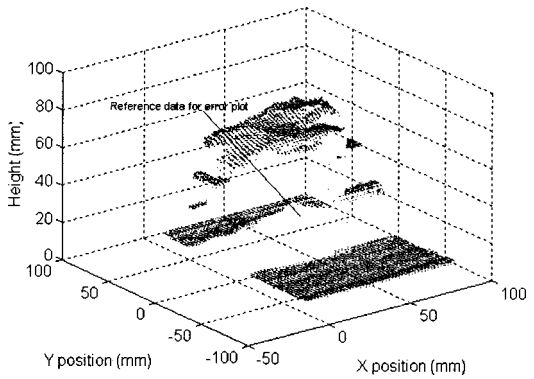

Fig. 18 Nugget mapped profile.

The system was implemented and tested on a 166-MHz Pentium computer, using the C++ programming language. The control code is interrupt driven. The computer system multitasks between two programs: a slow outer loop (which handles subsystem task scheduling and interaction of the system with the user), and a faster time-critical inner control loop (which processes the encoder information and produces an output control commands for the manipulator/gripper and the vision systems). Information is passed between the two loops via data latching and semaphore. Since the outer loop can be interrupted at any time, including while writing data to memory, it is necessary to set up strict guidelines about the validity of data being transferred between the two programs. This is an added complication inherent in multitasking or parallel processing.

Since the crucible charging environment can be damaged rather easily, it is very important to allow user interaction to alter the manipulator's behavior on-line. The system is able to pack nuggets at an average rate of 1 nugget every 10 seconds, reaching a charge density of 50% for the 45.7-cm-diam crucibles, allowing the system to stay competitive with human packing.[1,2]

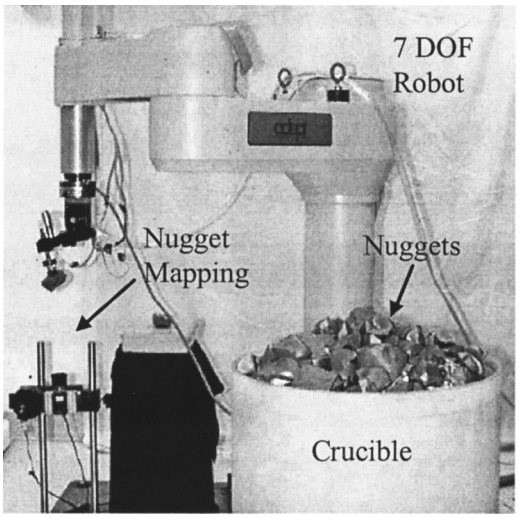

Fig. 20 Experimental system.

6 Conclusions

The technology has been developed to enable the robotic packing of crucibles in CZ semiconductor wafer production. Benefits of the system include elimination of nonergonomic working conditions, shorter crucible packing times, greater crucible packing consistency, and higher productivity and reduced costs.[1] A vision system to provide visible surface geometries of individual nuggets and nuggets packed in the crucible is a key component of this system.

An optical 3-D surface geometry measuring system has been developed based on active laser triangulation. It is found to be within the design constraints of the CZ application. It measures the geometry profile of the individual nuggets being placed and the landscape of the nuggets already in the crucible, with a resolution of 1 mm and scanning times of 2.5 and 4.5 s, respectively, with a nominal data acquisition rate of 15 KHz. While this speed can be increased relatively directly by low cost improvements in the basic system hardware, this is sufficient to meet the packing system requirements. This study shows that a practical and effective vision system can be designed to perform important and realistic industrial tasks. The integrated system has achieved charge densities of about 50% for 45.7-cm-diam crucibles. Required precision with cost constraints has been demonstrated.

Acknowledgments

The technical and financial support of this work by Shin-Etsu Handotai Co. is acknowledged. Also the technical cooperation of Professor Y. Ohkami and his team at the Tokyo Institute of Technology is much appreciated.

References

1. V. A. Sujan, S. Dubowsky, and Y. Ohkami, ''Design and implementation of a robot assisted crucible charging system,'' *Proc. IEEE Intl. Conf. Robotics Automation*, **2**, 1969–1975, San Francisco, CA (Apr. 2000).
2. V. A. Sujan, S. Dubowsky, and Y. Ohkami, ''Robotic manipulation of highly irregular shaped objects: Application to a robot crucible packing system for semiconductor manufacture,'' *SME J. Manuf. Processes* **3**(3), in press (2002).
3. V. A. Sujan and S. Dubowsky, ''Application of a model-free algorithm for the packing of irregular shaped objects in semiconductor manufacture,'' *Proc. IEEE Intl. Conf. Robotics Automation*, **2**, 1545–1550, San Francisco, CA (Apr. 2000).
4. V. A. Sujan and S. Dubowsky, ''The design of a 3-D surface geometry acquisition system for highly irregular shaped objects: with application to CZ semiconductor manufacture,'' *Proc. IEEE Intl. Conf. Robotics Automation*, **2**, 951–956, Detroit, MI (May 1999).
5. S. Alkon, ''Measurement and inspection using non-contact electro-optical systems: non-contact gauging and measurement with laser triangulation,'' *Proc. SPIE* **1038**, 28–35 (1989).
6. G. Bazin, B. Journet, and D. Placko, ''General characterization of laser range-finder optical heads,'' *Proc. LEOS '96 9th Annual Meeting*, **1**, 232–233, IEEE Lasers and Electro-Optics Society, New York (1996).
7. P. J. Besl, ''Active optical range imaging sensors,'' *Mach. Vision Appl.* **1**(2), 127–152 (1989).
8. R. L. Dalglish, C. McGarrity, and J. Restrepo, ''Hardware architecture for real-time laser range sensing by triangulation,'' *Rev. Sci. Instrum.* **65**, 485–491 (1994). .
9. J. A. Davis, E. Carcole, and D. M. Cottrell, ''Range-finding by triangulation with nondiffracting beams,'' *Appl. Opt.* **35**, 2159–2161 (1996).
10. R. A. Jarvis, ''A perspective on range finding techniques for computer vision,'' *IEEE Trans. Pattern Anal. Mach. Intell.* **PAMI-5**(2), 122–139 (1983).
11. B. Journet and G. Bazin, ''Laser range-finding techniques for industrial applications,'' *28th Int. Smp. Automotive Technol. Automation*, pp. 369–376, Dedicated Conf. Robotics, Motion and Machine Vision in the Automotive Industries, Automotive Automation Ltd., Croydon, UK (1995).
12. S. Monchaud, ''Contribution to range finding techniques for third generation robots,'' *Intell. Autonomous Syst.*, pp. 459–469, North-Holland, Amsterdam, Netherlands (1987).
13. R. G. Rosandich, *Intelligent Visual Inspection*, 1st ed., Chapman and Hall, London (1997).
14. T. A. Bossiuex, *Integration of Vision and Robotic Workcell*, American Institute of Aeronautics and Astronautics Publication, AIAA-94-1186-CP, Ford Motor Company (1993).
15. W. J. Hsueh and E. K. Antonsson, ''An optoelectronic and photogrammertric 3-D surface geometry acquisition system,'' ASME Winter Annual Meeting on Instrumentation and Components for Mechanical Systems, EDRL-TR92a (Nov. 1992).
16. T. Kanade, H. Kano, S. Kimura, A. Yoshida, and K. Oda, ''Development of a video-rate stereo machine,'' *Proc. Intl. Robotics Syst. Conf.* (IROS'95), August 5–9, Pittsburgh, PA (1995).
17. K. A. Tarabanis, P. K. Allen, and R. Y. Tsai, ''A survey of sensor planning in computer vision,'' *IEEE Trans. Rob. Autom.* **11**, 86–104 (1995).
18. Y. Tanaka, A. Gofuku, and M. Abdellatif, ''Video-rate 3-D range finder using RGB-signals from binocular cameras,'' *Proc. Fourth IASTED Intl. Robotics Manuf.*, pp. 166–168, IASTED-Acta Press, Anaheim, CA (1996).
19. R. C. Luo and R. S. Scherp, ''3D object recognition using a mobile laser range finder,'' *IEEE Intl. Workshop Intell. Robots Syst.* IROS'90, 673–677 (1995).
20. M. Rioux, ''Laser range finder based on synchronized scanners,'' *Appl. Opt.* **23**(21), 3837–3844 (1984).
21. E. Hecht, *Optics*, 2nd ed. Addison Wesley, Reading, MA (May 1990).
22. R. Holmes and C. Cummings, ''How to choose the proper illumination source,'' *Techspec* **3** (1997-1998).

Vivek A. Sujan received his BS in physics and mathematics *summa cum laude* from the Ohio Wesleyan University in 1996, his BS in mechanical engineering with honors, from the California Institute of Technology, 1996, and his MS in mechanical engineering from the Massachusetts Institute of Technology in 1998. He is currently completing his PhD in mechanical engineering at M.I.T. Research interests include the design, dynamics, and control of electromechanical systems; mobile robots and manipulator systems; optical systems and sensor fusion for robot control; and image analysis and processing. He has been elected to Sigma Xi (Research Honorary Society), Tau Beta Pi (Engineering Honorary Society), Phi Beta Kappa (Senior Honorary Society), Sigma Pi Sigma (Physics Honorary Society), and Pi Mu Epsilon (Math Honorary Society).

Steven Dubowsky received his bachelor's degree from Rensselaer Polytechnic Institute of Troy, New York, in 1963, and his MS and ScD degrees from Columbia University in 1964 and 1971. He is currently a professor of mechanical engineering at M.I.T. He has been a professor of engineering and applied science at the University of California, Los Angeles, a visiting professor at Cambridge University, England, and a visiting professor at the California Institute of Technology. During the period from 1963 to 1971, he was employed by the Perkin-Elmer Corporation, the General Dynamics Corporation, and the American Electric Power Service Corporation. His research has included the development of modeling techniques for manipulator flexibility and the development of optimal and self-learning adaptive control procedures for rigid and flexible robotic manipulators. He has authored or coauthored nearly 100 papers in the area of the dynamics, control, and design of high performance mechanical and electromechanical systems. He is a registered Professional Engineer in the State of California and has served as an advisor to the National Science Foundation, the National Academy of Science/Engineering, the Department of Energy, and the US Army. He has been elected a fellow of the ASME and is a member of Sigma Xi and Tau Beta Pi.